To be submitted to *Analytical Chemistry*

Quantitative image analysis of broadband CARS microscopy hyperspectral images of polymer blends

Young Jong Lee[*]*, Doyoung Moon, Kalman B. Migler, and Marcus T. Cicerone*[*]

Polymers Division, National Institute Standards and Technology, Gaithersburg, Maryland, USA

Email addresses: yjlee@nist.gov, cicerone@nist.gov.

We demonstrate that broadband coherent anti-Stokes Raman scattering (CARS) microscopy can be very useful for fast acquisition of quantitative chemical images of multilayer polymer blends. Since a raw CARS signal results from coherent interference of resonant Raman and nonresonant background, its intensity is not linearly proportional to the concentration of molecules of interest, and it is challenging to perform a quantitative image analysis of a CARS image. Here we have developed a sequence of data processing steps to retrieve background-free and noise-reduced Raman spectra over the whole frequency range including both the fingerprint and C-H regions. Using a classical least squares approach, we are able to decompose a Raman hyperspectral image of a tertiary polymer blend into quantitative chemical images of individual components. We use this method to acquired 3-D sectioned quantitative chemical images of a multilayer polymer blend of polystyrene/styrene-ethylene-propylene-copolymer/polypropylene.

[1]Raman microscopy has been widely used to acquire label-free chemical imaging of soft and complex materials including polymeric and biological samples. However, major weaknesses of conventional spontaneous Raman imaging methods include weak signal intensity and an often strong fluorescence background in the same spectral range as the Raman signal. Many nonlinear Raman methods have been developed to enhance the Raman signal. Successful applications for microscopy include coherent anti-Stoke Raman scattering (CARS) microscopy[1,2] and Raman gain/loss microscopy.[3] In both cases, single frequency (narrow spectral bandwidth) approaches have been widely used to take advantage of high scanning speed. However, single frequency approaches do not facilitate extraction of quantitative composition information from samples with overlapped spectral peaks. On the other hand, in multiplex or broadband hyperspectral imaging, one obtains a Raman spectrum at each spatial pixel, and quantitative analysis of complex samples is possible. While multiplex Raman gain/loss microscopy has not been demonstrated as a useful imaging modality yet due to limited dynamic range of current multiplex detection systems,[4] broadband CARS has been fairly well developed and proven as a robust imaging tool. Broadband CARS signal is generated by overlapping a narrowband pulse with a pulse from a femtosecond oscillator or from a continuum source.[5] The CARS signal is generated at higher frequency than any of the input pulses, so there is no interference from fluorescence generated by single-photon processes. Because the CARS process is nonlinear, signal is generated only at the focal point where the multiphoton process is most enhanced, leading to 3-D sectioning capability.

The CARS signal intensity is dramatically enhanced compared to spontaneous Raman scattering under conditions common to materials imaging. However, a non-resonant background (NRB) accompanies the resonant CARS signal, and very often dominates the weaker resonant signals of interest. The NRB in CARS interferes coherently with the resonant signal resulting in a dispersive line shape and amplitude, making quantitative analysis difficult. Many sophisticated optical schemes have been devised to minimize the NRB contribution to the measured CARS spectrum.[6-10] However, in each case overall CARS signal strength is sacrificed, which can adversely affect the signal-to-noise (S/N) ratio of the detected CARS spectrum. Alternatively, computational methods have been demonstrated to retrieve the resonant signal of interest from the NRB in multiplex or broadband CARS spectra.[11-14] Unlike other approaches based on iterative fitting,[11-13] we use a modified Kramers-Kronig (KK) transform method[14] to extract resonant Raman-equivalent spectra from raw CARS spectra and a separately measured NRB spectrum in a straightforward way without iterative fitting. This KK method has been used to retrieve weak Raman signal from a biological sample rapidly.[14,15] Here, we applied broadband CARS microscopy to acquire 3-D quantitative chemical images of 2- and 3-component multilayer polymer blends.

The blending of immiscible polymers by melt mixing is widely used to produce materials with tailored properties. Controlling specific structures during the mixing processes makes new physical, chemical, and biological properties available. For example, a multi-layer structure can reduce gas transport,[16] a co-continuous structure of a polymer scaffold can be used for tissue engineering,[17] and a domain/matrix structure can be used to control mechanical properties such as brittleness.[18] The planar polymer micro-mixer (PPMM) is a novel microfluidic polymer melt mixer that is useful for the case of a limited amount of sample (tenth of mg) or requiring the

forced mixing of immiscible polymers for the targeted structures such as multilayer, co-continuous, domain/matrix and multiple coaxial structure.[19,20]

Polymer blend structures are often imaged at high spatial resolution using scanning electron microscopy (SEM) and tunneling electron microscopy (TEM).[21] These methods generally do not provide chemical phase information, so auxiliary methods such as solution extraction are frequently used.[22] Solution extraction is not amenable for use with multilayer blends due to potential for destruction of the original morphology during solution extraction. Therefore, sample cross sections of multilayer blends are typically prepared for SEM analysis by cryo-fracture,[19] where chemical contrast is derived from differences in texture of broken surfaces. For TEM analysis, additional heavy metal staining is necessary for chemical image contrast.[21] These electron microscopy techniques require complicated and invasive sample preparation procedures and it is very challenging to obtain reliable spatio-chemical information with only SEM/TEM analysis.

We demonstrate that broadband CARS microscopy can be used to acquire 3-D sectioned images of all chemical components noninvasively, without the additional sample preparation steps required for electron microscopy imaging. We perform quantitative image analysis of Raman spectra of both the fingerprint and C-H regions using a classical least square approach after the CARS spectra have been de-noised using singular value decomposition and transformed into background-free Raman spectra using a modified Kramers-Kronig phase retrieval and baseline detrending. We apply this noninvasive optical approach to study compatibilizer effects in structure morphology evolution of chemical species in a tertiary polymer blend.

EXPERIMENTAL SETUP

Sample Preparation. [2]The PPMM was designed for high temperature operation, mechanical simplicity, cleanability and optical access, as described in detail elsewhere.[19] It consists of a steel sample holder (the top plate), a stack of three laser-cut stainless steel shims (25 or 50 μm in thickness each), and a sapphire window (the bottom plate). The operating temperature was kept at 207 ºC during the mixing process, and the inlet pressure was controlled by a linearly increasing profile (up to 7 MPa) to maintain a constant averaged flow rate through the successive mixing SAR units. Nitrogen was used to drive the molten polymer into the flow channels, and the flow pattern was viewed and video-recorded through the sapphire window. The hot polymer blend was slowly cooled down in the air before it was detached from the mixer for further analysis. Briefly, as shown in Fig. 1(a), the three-component PPMM consists of the entrance region and a series of the split and rejoining (SAR) region. At the entrance region, the components A and C form a parallel flow in one "T" junction and the components B and C form another parallel flow in the other "T" junction. The two parallel flows of C/A and C/B join at another "T" junction to form a parallel flow of four layers with a C/A/C/B sequence. The thickness of the flow channel inlet for the component C is 50 μm while the thickness of the other channels for the components A and B are 75 μm. This parallel flow enters a series of SAR units, where the layered flow is split into two perpendicular channels and recombined into one channel by placing one split stream on top of the other. As the layered flow passes *n* SAR units, the number of layers in the flow increases by 2^n. The width of the mixing channel is 750 μm and the

[2] Certain equipment, instruments or materials are identified in this paper in order to adequately specify the experimental details. Such identification does not imply recommendation by the National Institute of Standards and Technology nor does it imply the materials are necessarily the best available for the purpose.

depth varies from 50 μm (split and reorientation region) to 125 μm (recombination region), which is determined by the combination of the top and bottom shims (50 μm in thickness) and the middle shim (25 μm in thickness). Polystyrene (PS, Styron 666D, DOW Chemical), polypropylene (PP, Exceed 4062, Exxon) and poly(styrene-ethylene/propylene) diblock copolymer (SEP, Kraton G 1701, Shell Chemical) were used as received.

For SEM imaging, the molded strip was detached manually from the shims, embedded into epoxy for a supporting medium. Then, the sample was frozen by liquid nitrogen and broken at target locations. The cross sections prepared by the cryo-fracture method were imaged by a scanning electron microscope (SEM; Hitachi, S-4700).

Broadband CARS Imaging. The experimental setup of the broadband CARS has been described previously.[15,23] Briefly, as shown in Fig. 1(b), the output (70 fs, centered at 830 nm, 80 MHz) of a Ti:S laser oscillator (MaiTai-DeepSee, Spectra-Physics) was split into two parts. One part was introduced into a photonic crystal fiber (Crystal Fibre, Femtowhite) to generate a continuum pulse. The continuum pulse spectrum was adjusted with an 850 nm longpass filter. The bandwidth of the remaining oscillator output (the narrowband pulse) was reduced by adjusting slit width in a 4-*f* dispersionless filter to 10 cm^{-1} full-width-half-maximum (FWHM). The two beams were introduced collinearly and with parallel polarization into a 60X 1.35 NA oil immersion objective lens (Olympus) and focused on the sample. The CARS signal generated from the sample was collected in the forward direction and passed through a set of an 830 nm notch filter and an 810 nm shortpass filter and was analyzed using a charge-coupled device (CCD; DU920-BR-DD, Andor) attached to a monochromator (SP-2300, Acton) with a grating with a groove density of 300 groove/mm. The spatial resolution was laterally 500 nm and axially 1 μm at the glass coverslip surface and became larger as the focus moves into a polymer sample due to spherical aberration. The average laser power at the sample was controlled below 10 mW

and 10 mW for the continuum and narrowband pulses, respectively, to avoid photodamage. The CCD exposure time is typically 20 ms or 50 ms per pixel.

Multivariate Image Analysis. The broadband CARS image data were acquired in the (x, z, ω) matrix at each y section, where the z-axis is normal to layer interfaces, the y-axis is parallel to the flow direction, the x-axis is perpendicular to the y- and z-axes, and ω indicates the Raman shift frequency dimension. Singular value decomposition (SVD) was performed using a user-built code based on LabView (National Instruments). The Kramers-Kronig phase retrieval[14] and baseline detrending processes were also performed using the same user-built LabView code. The retrieved Raman spectral image of a polymer blend was analyzed with a classical least square (CLS) method by a commercial package for multivariate image analysis (Solo + MIA, Eigenvector). The Raman spectra of pure components were used as basis functions for the CLS analysis.

RESULTS AND DISCUSSION

The SEM images in Figs. 2(a) and 2(b) show layer structures with a high spatial resolution, sufficient to provide detailed texture of the cross section surfaces. In particular, the SEM images of the cryo-fractured cross section show clear difference in texture among the layers. Limited chemical identification of the individual layers was achieved by comparing with the textures of identifiable regions of the same or other cross sections. SEM images allow for precise measurement of physical dimensions and observation of structural morphology. However, the cryo-fracturing technique requires very careful sample handling to achieve a cross section at a desired location in a small micro-mixer sample, but more importantly, it is impossible to obtain multiple cross sections separated by well defined distances, which is crucial for studying morphology evolution along the flow direction in forced assembly mixers. Alternatively, a

microtome method can provide multiple cross sections separated by well-controlled distances. However, image contrast is significantly reduced in the SEM image of the microtomed surface, as shown in Fig. 2(b), where it is almost impossible to recognize even the layer boundaries. The loss of fine texture used for image contrast makes the microtome method not applicable for conventional SEM imaging of layered polymer blends. In addition, embedded epoxy for support during cryo-fracturing or microtoming can potentially alter morphology of a multilayer polymer blend.

We acquired CARS image data of a PS/PP PPMM blend at three optical cross sections separated by 5 μm without any additional sample preparation steps. The CARS spectra look very different between two regions and are easily identifiable as PS and PP, as shown in Fig. 2(f). PS is characterized by the phenyl ring breathing mode at 1000 cm^{-1} and the C-H stretching mode on the phenyl ring at 3100 cm^{-1}, while PP is characterized by the strong CH_2 and CH_3 modes at 2800 - 2900 cm^{-1}. The false color images are constructed at the frequencies of 990 cm^{-1} (red) and 2880 cm^{-1} (green), which represent the frequencies of the most intense CARS peaks of PS and PP, respectively. The images show clear layer structure of PS and PP, with some delamination and cracks within layers. However, as mentioned above, the NRB contribution, which appears as a slowly varying baseline in the CARS spectra of Fig. 2(f), prevents quantitative chemical analysis of the CARS images. Due to the peak shift and the nonlinear dependence on concentration, caused by the NRB interference, single frequency-based image analysis cannot provide quantitative information.

To construct quantitative Raman images, we performed a series of data processing steps: (1) singular value decomposition (SVD); (2) modified Kramers-Kronig (KK) phase retrieval; (3) baseline detrending (BD); and (4) classical least square (CLS) analysis. All the data processes require multiplexed spectra, and are not applicable to single-frequency based CARS microscopy.

Singular Value Decomposition (SVD). The SVD method has been used as an extremely powerful means to reduce noise from hyperspectral images.[24] SVD factors a (m × n)-matrix **D** into a product of three matrix factors, $\mathbf{D} = \mathbf{USV}^T$. For CARS hyperspectral image data, the original data matrix **D** is arranged as ($\omega \times xy$), where ω is the number of frequency elements and *xy* indicates the product of *x* and *y* image pixels. The matrix **U** contains the so-called basis spectra, **V** is a matrix containing the amplitude vectors as an image, and **S** is a diagonal matrix containing the singular values. Some of the spectral and spatial vectors in **U** and **V** are dominated by random noise. Removing only those noise dominating components will reduce noise without losing information of interest. Mathematically, one can transform **S** into a reduced matrix **S**' by replacing singular values corresponding to random noise with zeros. The reconstructed **D**' from $\mathbf{D}' = \mathbf{US}'\mathbf{V}^T$ will contain noise-reduced spectral information of interest. The challenge in using SVD is to objectively decide on which singular values are statistically and physically significant. Several numerically-based criteria have been used to determine which singular values to keep for SVD reconstruction. For example, the criteria used in Ref. [25] are (i) distinctive change in declining slope of singular values; (ii) the first-order autocorrelation function for columns of the **U** and **V** matrices; and (iii) the randomness of residual plots for the difference between the original **D** and a reconstructed **D**' calculated with trial singular values. These criteria were demonstrated to be useful for spectral noise reduction of UV spectra of DNA melting profiles.[25] Validity of those criteria for our broadband CARS analysis are tested by using an example of CARS hyperspectral data of a PS/SEP/PP polymer blend with 569 frequency elements and 101×141 image pixels. There is no distinctive change in the change of slope for the singular values shown in Fig. 3(b), so criterion (i) does not provide an unambiguous metric. Applying criterion (ii) to the first-order autocorrelation functions plotted in Fig. 3(c), leads to use of either the first two or the first seven singular values, depending on whether columns of the **U** or **V**

matrices are used for the autorrelation. We reconstructed new **D**' using two and seven singular values and generated the residual matrices (**D** - **D**') as suggested by the criterion (iii). The images of residual matrixes (**D** - **D**') with singular values of two and seven, shown in Figs. 3(d) and 3(e), respectively, exhibit noticeable structural features, indicating that the numerical criteria can cause loss of meaningful physical information through SVD filtering. The excessive truncation for **S**' with the numerical criterion (ii) must be related with the characteristics of the hyperspectral image data: for the **U** matrix, sharp spectral peaks will cause the first-order autocorrelation function to be underestimated; and similarly for the **V** matrix, small features compared with pixel-to-pixel distance will be regarded as noise in the first-order autocorrelation consideration.

Therefore, we use a rather qualitative criterion based on randomness of images of the individual columns of **V** and confirm whether to determine the significance of their corresponding singular values. Figure 3(a) shows the images of the matrix **V** columns corresponding to the first 20 singular values of the CARS image of a PS/SEP/PP polymer blend. Among them, 13 images are selected to be meaningful based on recognition of meaningful features by the user. It is clear that the reconstructed image of the residual matrix (**D** - **D**') of Fig. 3(f) contains mostly random noise, compared with Figs. 9(a) and 9(b).

Figure 4 shows spectra at various stages of data processing for PS and PP CARS spectra measured from 50 μm thick homopolymers located on a glass coverslip. Figure 4(a) shows raw CARS spectra of single spatial pixels taken from CARS images with 101x101 pixels and 622 frequency elements. As shown in Fig. 4(b), application of the SVD filtering process with the criterion based on the **V** column images allows significant reduction of spectral noise with minimal loss of meaningful spectral information.

Kramers-Kronig (KK) Phase Retrieval And Baseline Detrending (BD). The CARS signal intensity is proportional to the squared modulus of the complex third-order susceptibility, $|\chi(\omega)|^2$, where $\chi(\omega)$ contains a resonant (χ_R) and nonresonant (χ_{NR}) part:

$$|\chi(\omega)|^2 = |\chi_{NR}(\omega)|^2 + 2\chi_{NR}\,\mathrm{Re}[\chi_R(\omega)] + |\chi_R(\omega)|^2$$

A modified Kramers-Kronig relation is used to retrieve the resonant Raman spectrum from the total CARS spectrum $|\chi(\omega)|^2$ and the nonresonant spectrum $|\chi_{NR}(\omega)|^2$, as described in detail previously.[14] A separately measured CARS spectrum of a glass coverslip is used as a nonresonant spectrum in the KK process. Figure 4(c) shows the KK-retrieved Raman spectra from the SVD-filtered CARS spectra of PS and PP and the SVD-filtered NRB spectra from the glass coverslip in the same measurements. While a total CARS signal is not proportional to sample concentration, a Raman signal in a KK-retrieved spectrum is linearly proportional to the concentration of molecules of interest, making quantitative data analysis possible.

The KK-retrieved Raman signal contains a slowly varying baseline. This is particularly evident in the region around 2000 cm^{-1}, where the signal is non-zero although there are no resonant peaks. The KK algorithm assumes that the reference NRB is identical to the NRB generated in the sample, and the presence of the nonzero baseline simply indicates that NRB associated with the sample is not the same as that measured in the glass. Currently we have no way to measure the CARS and NRB spectra simultaneously at the same sample location. A simple and practical way to remove the baseline is to subtract a baseline determined by polynomial fitting over three Raman quiescent regions in the KK retrieved spectrum. Figure 4(d) shows the KK-retrieved Raman spectra of PS and PP after baseline detrending (BD).

We now turn to analysis of the retrieved Raman spectra. If each chemical component was associated with a unique Raman peak, it would be straightforward to discriminate the chemical components of essentially any blend by simply quantifying the amplitude of each identifying

peak at each spatial pixel. Such a simple analysis is not possible for our PS/SEP/PP blend, however. As shown in Fig. 5(a), SEP, used as compatibilizer, is co-polymer including both styrene (the monomer unit of PS) and propylene (the monomer unit of PP) units. All Raman peaks from SEP are also shared by either PS or PP, as shown in Fig. 5(b). We attempt a simple spectral analysis, the results of which are shown in the false color image of Fig. 5(c). This image was constructed using contrast from peaks at frequencies of 1000 cm^{-1} (red), 2880 cm^{-1} (green), and 2850 cm^{-1} (blue) for PS, PP, and SEP, respectively. Line scans at the indicated location in Fig. 5(c) are normalized with the maximum intensities and plotted to represent the fraction of each component. The sum of individual line scans is larger than 1.5 at most of the region, indicating that the image constructed Raman intensity at single frequencies is not properly calibrated. As expected from the spectral overlap shown in Fig. 5(b), the single-frequency image analysis can provide qualitative information on which chemical components are dominant but cannot provide quantitative information about how much the chemical components are present.

Classical Least Square (CLS) Analysis. We applied a multivariate approach to analyze the hyperspectral data quantitatively. Among many different multivariate regression methods, classical least square (CLS) is the most often used to determine the concentrations (a_i) of multiple components (i) from a mixture spectrum, $\Phi(\omega) = \sum a_i \phi_i(\omega) + E(\omega)$,[26] where $E(\omega)$ is the error, when the individual spectra, $\phi_i(\omega)$, of all of the pure components are known. We use separately measured pure Raman spectra of PS, PP, and SEP homopolymers, shown in Fig. 5(b), to perform CLS analysis using the pure spectra to determine concentrations (a_i) or fractions of the three components at each image pixel. Figure 5(d) shows a false color image of the a_i for the three components determined with CLS analysis. As the line scan of Fig. 5(f) shows, the concentrations of all three components range from zero to one and the sum is close to unity, indicating the fractions a_i are complementary. This result supports the idea that the CLS

multivariate analysis can provide quantitative information of the 3-D chemical image by broadband CARS hyperspectral data.

It should be noted that several optical artifacts can cause errors in a quantitative CLS. These artifacts include spherical aberration and sample scattering. Spherical aberration caused by refractive mismatch of the sample and a glass coverslip increases as the focus moves farther from the surface of the glass coverslip and he reduced effective light intensity at the focus will lower nonlinear CARS signal intensity. Similarly, the CARS signal will be reduced as the focus moves deeper from the sample entrance surface in a turbid sample . The *z*-dependent deviation can be seen in Fig. 5(f), the sum of the spectral components becomes smaller as the *z* value increases, that is, as the focus moves farther from the entrance. This is simply due to diminished signal level at increased depth. In principle this reduced signal level could be corrected. These artifacts notwithstanding, multivariate image analysis of broadband CARS images provides a much better quantitation than can be achieved with single-frequency based image acquisition or analysis.

Figure 6 shows quantitative chemical images of the third and fourth SAR segments at separated optical cross sections of the PS/SEP/PP blend. The 3-D sectioned images of the third segment look very different from the images of the fourth segment. The breakdown stage of the laminar phase is different from that of the equivalent PS/PP PPMM blend, which occurs at the sixth segment from Ref. [27], which discusses the effect of the compatibilizer, SEP, and relative viscosities among three polymer components on morphology evolution in a PPMM blend. Their results indicate that the viscosity ratio of the compatibilizer relative to the other polymers controls the multilayer stability (earlier breakdown of the layered morphology) during flow while its reduced interfacial tension controls the final domain size.[27]

It can be noted that the volume of SEP in the images of Figs. 5 and 6 is much smaller than that of PS and PP. The flow rate must be proportional to the cross section of the inlet channel and be inversely proportional to the viscosity of the fluid when the same inlet pressure is applied for all components. The height of the SEP channel (50 μm) is lower than those of the PS and PP channels (75 μm). In addition, separate viscosity measurements[27] of the same polymer stocks show that the viscosity of SEP (60,000 Pa s) is about three times larger than that of PS (15,000 Pa s) or PP (20,000 Pa s) at the mixing temperature (207 °C). Therefore, both the smaller cross section and higher viscosity of the SEP are consistent with the small volume fraction of the SEP component.

CONCLUSIONS

We have demonstrated that broadband CARS can be used to acquire quantitative chemical images of polymer blends. This nonlinear optical imaging method based on Raman scattering provides 3-D sectioned chemical information without the additional sample preparation steps, such as staining or fracturing, which are required for conventional electron microscopy imaging. The CARS hyperspectral data of multilayer polymer blends were transformed into background-free Raman spectral data with singular value decomposition, Kramers-Kronig phase retrieval, and baseline detrending, and then a multivariate analysis method (classical least square) was used to decompose the whole Raman spectra into the sum of each chemical component and to construct a quantitative chemical image of each component. We have discussed the location of the compatibilizer, SEP, in a PS/SEP/PP blend and to study the compatibilizer effect on morphology evolution of the polymer mixing.

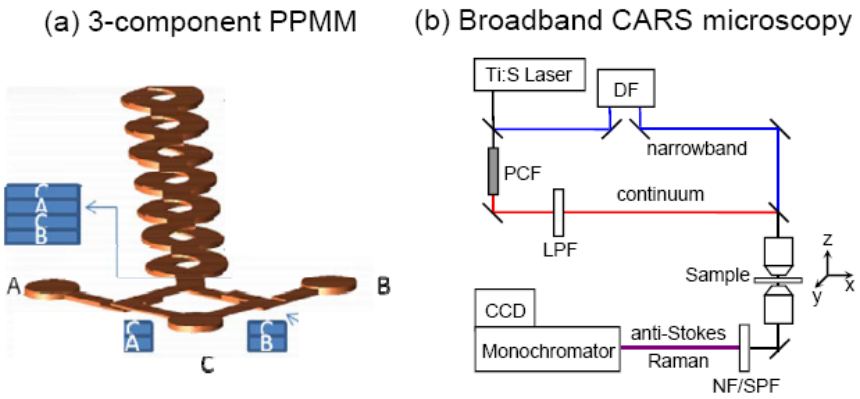

Figure 1. (a) Schematic diagram of the three-component planar polymer micro-mixer (PPMM). (b) Schematic diagram of broadband coherent anti-Stokes Raman scattering (CARS) microscopy. PCF: photonic crystal fiber; DF: dispersionless filter; LPF: long-pass filter; NF: notch filter; and SPF: short-pass filter. In this paper, the y-axis is parallel to the flow direction; the z-axis is the normal direction of the layers; and the x-axis is perpendicular to the y- and z-axes.

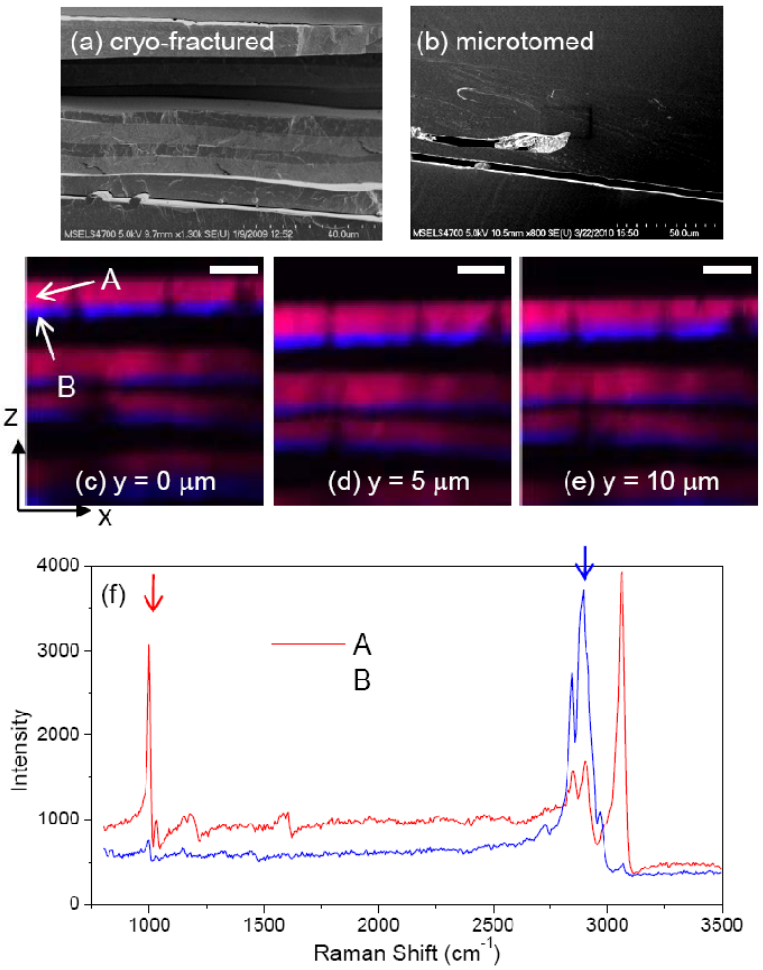

Figure 2. SEM images of (a) cryo-fractured and (b) microtomed cross sections of a PS/PP PPMM blend prepared at the third SAR segments. (c)-(e) CARS hyperspectral image of an optical cross section at the third segment of PS/PP blend prepared by PPMM. The raw CARS data was used to construct the false color image, where the red and blue color indicates the intensity at 990 cm^{-1} and 2880 cm^{-1}, respectively. (f) The CARS spectra measured at the locations A and B, as indicated in the first image. The scale bar in the CARS images indicates 20 μm. The 40x 0.95 NA objective lens was used. The exposure time was 50 ms.

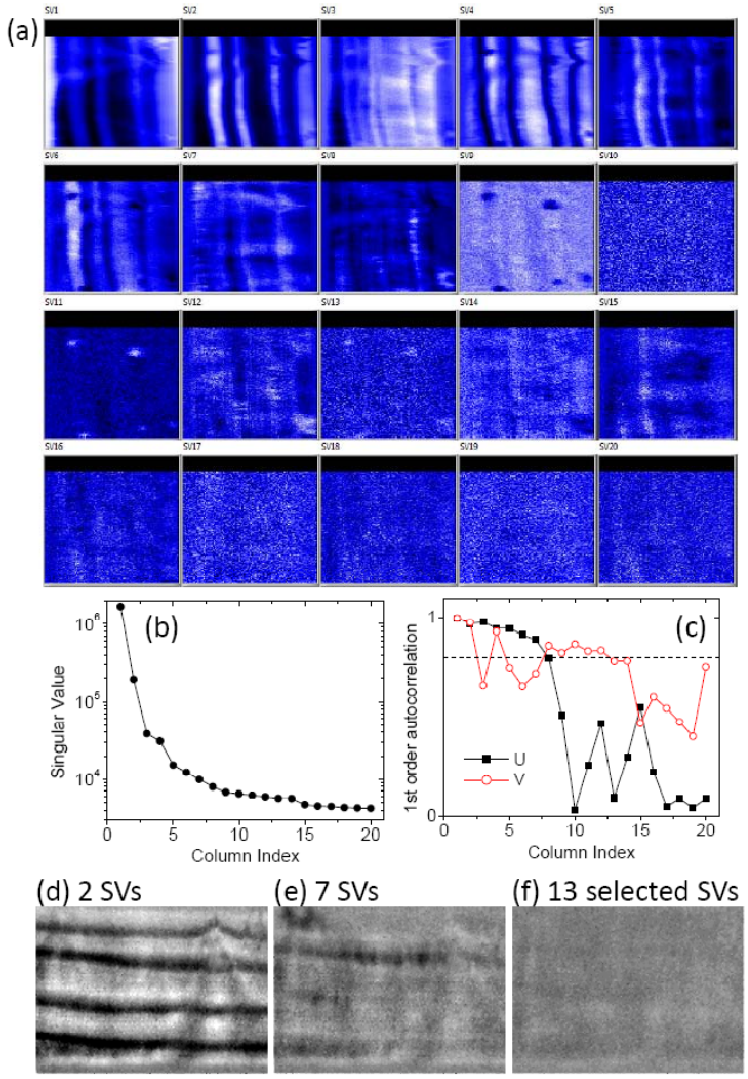

Figure 3. Singular value decomposition (SVD) of CARS hyperspectral data of a PS/SEP/PP blend. (a) The images of the first 20 columns of the generated **V** matrix. (b) Plot of singular values in the matrix **S**. (c) The normalized first-order autocorrelation function of the columns of the **U** and **V** matrices. (d)-(f) Total spectral intensity images of the residual matrix (**D** - **D**') generated with various number of singular values determined by different criteria (described in text). For the residual image (f), thirteen singular values (indices of 1 through 9, 11, 12, 14, and 15) are used as nonzero to reconstruct **S**' and **D**'.

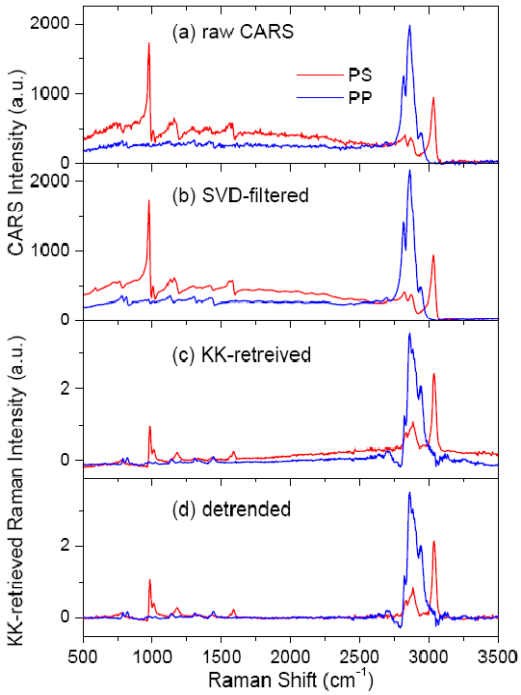

Figure 4. Examples of data processing of CARS spectra taken from PS and PP homopolymers. (a) The raw CARS spectra were taken by single measurements for 20 ms exposure time. (b) The SVD filtering was performed over 101x101 pixels for a CARS hyperspectral image of a homopolymer layer on a glass coverslip. The singular values were four and five for PS and PP, respectively, following the criteria explained in the text. (c) The KK-retrieval was performed for the SVD-filtered CARS spectra with the SVD-filtered NRB spectra measured from the glass coverslip. (d) The KK-retrieved spectrum was subtracted by a baseline determined by fitting it with a fourth-order polynomial over three separate frequency regions where Raman resonance is absent (500 - 600 cm^{-1}, 1600 - 2600 cm^{-1}, and 3250 - 3500 cm^{-1}).

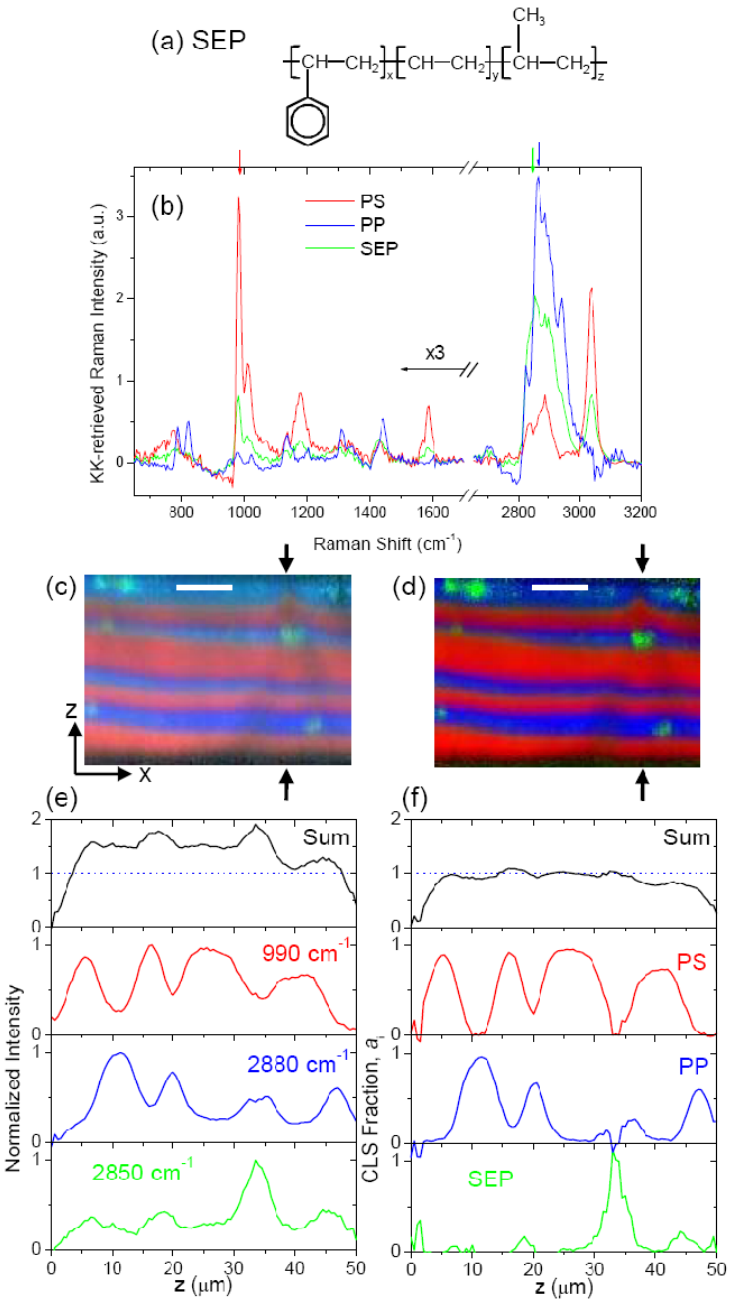

Figure 5. (a) Chemical structure of SEP. (b) Raman spectra generated with SVD, KK, and BD from CARS data of PS, SEP, and PP homopolymers. For (c)-(f), CARS hyperspectral data were acquired from a PS/SEP/PP PPMM blend at the third segment, and the data were processed with SVD, KK, and BD in sequence. Then, the false color image (c) was constructed by single-frequency intensities at 990 cm^{-1} (red), 2890 cm^{-1} (blue), and 2850 cm^{-1} (green). Then, the image

data were processed with CLS using the pure component spectra of (b). The false color image (d) was constructed by the fractions determined by CLS: PS (red), PP (blue), and SEP (green). The scale bar indicates 20 μm. The exposure time was 50 ms.

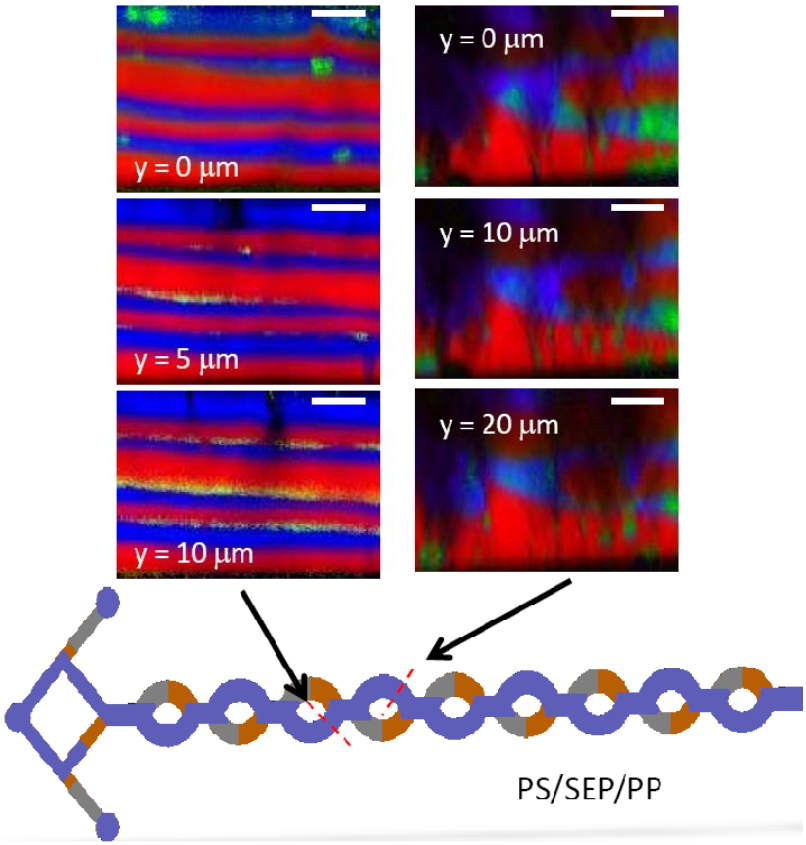

Figure 6. 3-D sectioned CARS images at the third and fourth segments of PS/SEP/PP blends. All the hyperspectral data were processed with SVD, KK, and BD, and the resulting CLS fractions were used for image construction. The false colors represent PS (red), PP (blue), and SEP (green), respectively. The scale bar indicates 20 µm. The exposure time was 50 ms.

References

(1) Zumbusch, A.; Holtom, G. R.; Xie, X. S. *Phys. Rev. Lett.* **1999**, *82*, 4142-4145.

(2) Evans, C. L.; Potma, E. O.; Puoris'haag, M.; Cote, D.; Lin, C. P.; Xie, X. S. *Proc. Natl. Acad. Sci. USA* **2005**, *102*, 16807-16812.

(3) Freudiger, C. W.; Min, W.; Saar, B. G.; Lu, S.; Holtom, G. R.; He, C. W.; Tsai, J. C.; Kang, J. X.; Xie, X. S. *Science* **2008**, *322*, 1857-1861.

(4) Ploetz, E.; Laimgruber, S.; Berner, S.; Zinth, W.; Gilch, P. *Appl. Phys. B-Lasers Opt.* **2007**, *87*, 389-393.

(5) Kee, T. W.; Cicerone, M. T. *Opt. Lett.* **2004**, *29*, 2701-2703.

(6) Cheng, J. X.; Book, L. D.; Xie, X. S. *Opt. Lett.* **2001**, *26*, 1341-1343.

(7) Cheng, J. X.; Volkmer, A.; Book, L. D.; Xie, X. S. *J. Phys. Chem. B* **2001**, *105*, 1277-1280.

(8) Lee, Y. J.; Cicerone, M. T. *Opt. Express* **2009**, *17*, 123-135.

(9) Oron, D.; Dudovich, N.; Yelin, D.; Silberberg, Y. *Phys. Rev. Lett.* **2002**, *88*, 063004.

(10) Sung, J.; Chen, B.-C.; Lim, S.-H. *J. Raman Spectrosc.* **2010**, in press.

(11) Rinia, H. A.; Bonn, M.; Muller, M.; Vartiainen, E. M. *Chemphyschem* **2007**, *8*, 279-287.

(12) von Vacano, B.; Meyer, L.; Motzkus, M. *J. Raman Spectrosc.* **2007**, *38*, 916-926.

(13) Liu, Y. X.; Lee, Y. J.; Cicerone, M. T. *J. Raman Spectrosc.* **2009**, *40*, 726-731.

(14) Liu, Y. X.; Lee, Y. J.; Cicerone, M. T. *Opt. Lett.* **2009**, *34*, 1363-1365.

(15) Parekh, S. H.; Lee, Y. J.; Aamer, K. A.; Cicerone, M. T. *Biophys. J.* **2010**, *99*, 2695-2704.

(16) Wang, H. P.; Keum, J. K.; Hiltner, A.; Baer, E.; Freeman, B.; Rozanski, A.; Galeski, A. *Science* **2009**, *323*, 757-760.

(17) Washburn, N. R.; Simon, C. G.; Tona, A.; Elgendy, H. M.; Karim, A.; Amis, E. J. *J. Biomed. Mater. Res.* **2002**, *60*, 20-29.

(18) Kyu, T.; Saldanha, J. M.; Kiesel, M. J. In *Two phase polymer systems*; Utracky, L. A., Ed.; Hanser Publ. Munich: New York, 1991, pp 259-275.

(19) Moon, D.; Migler, K. B. *Polymer* **2010**, *51*, 3147-3155.

(20) Schonfeld, F.; Hessel, V.; Hofmann, C. *Lab on a Chip* **2004**, *4*, 65-69.

(21) Radonjic, G. *J. Appl. Polym. Sci.* **1999**, *72*, 291-307.

(22) Lyngaaejorgensen, J.; Utracki, L. A. *Makromol. Chem. Macromol. Symp.* **1991**, *48-9*, 189-209.

(23) Lee, Y. J.; Parekh, S. H.; Kim, Y. H.; Cicerone, M. T. *Opt. Express* **2010**, *18*, 4371-4379.

(24) van Manen, H. J.; Kraan, Y. M.; Roos, D.; Otto, C. *Proc. Natl. Acad. Sci. USA* **2005**, *102*, 10159-10164.

(25) Haq, I.; Chowdhury, B. Z.; Chaires, J. B. *Eur. Biophys. J.* **1997**, *26*, 419-426.

(26) Seasholtz, M. B.; Archibald, D. D.; Lorber, A.; Kowalski, B. R. *Appl. Spectrosc.* **1989**, *43*, 1067-1072.

(27) Moon, D.; Lee, Y. J.; Cicerone, M. T.; Migler, K. B., to be submitted.